Magnetic and structural properties of GeMn films: precipitation of intermetallic nanomagnets

S. Ahlers, D. Bougeard, N. Sircar, and G. Abstreiter

Walter Schottky Institut
Technische Universität München
Am Coulombwall 3, D-85748 Garching, Germany

A. Trampert

Paul-Drude-Institut für Festkörperelektronik
Hausvogteiplatz 5-7, D-10117 Berlin, Germany

M. Opel and R. Gross

Walther-Meissner-Institut
Bayerische Akademie der Wissenschaften
Walther-Meissner-Str. 8, 85748 Garching, Germany
(Dated: February 6, 2008)

We present a comprehensive study relating the nanostructure of $Ge_{0.95}Mn_{0.05}$ films to their magnetic properties. The formation of ferromagnetic nanometer sized inclusions in a defect free Ge matrix fabricated by low temperature molecular beam epitaxy is observed down to substrate temperatures T_S as low as 70°C. A combined transmission electron microscopy (TEM) and electron energy-loss spectroscopy (EELS) analysis of the films identifies the inclusions as precipitates of the ferromagnetic compound Mn_5Ge_3. The volume and amount of these precipitates decreases with decreasing T_S. Magnetometry of the films containing precipitates reveals distinct temperature ranges: Between the characteristic ferromagnetic transition temperature of Mn_5Ge_3 at approximately room temperature and a lower, T_S dependent blocking temperature T_B the magnetic properties are dominated by superparamagnetism of the Mn_5Ge_3 precipitates. Below T_B, the magnetic signature of ferromagnetic precipitates with blocked magnetic moments is observed. At the lowest temperatures, the films show features characteristic for a metastable state.

PACS numbers: 61.46.Df, 75.50.Pp, 75.70.-i

I. INTRODUCTION

Magnetic semiconductors have attracted considerable technological as well as fundamental scientific interest. Research has been driven mainly by their possible applicability in spintronics devices. The GeMn material system is a promising candidate compatible to the widespread Si semiconductor technology. Various fabrication techniques have recently been employed to realise GeMn magnetic semiconductors, including single crystal growth,[1] solid phase epitaxy[2] and molecular beam epitaxy (MBE).[3,4,5,6,7,8,9] Irrespective of the fabrication technique, the formation of ferromagnetic, intermetallic compounds can occur. Bulk thin intermetallic films have been observed on Ge(111),[2] while phase separation was found on a μm scale in single crystals[1] and on a sub-μm scale in MBE fabricated samples.[9] Since the Mn content in ferromagnetic GeMn intermetallic compounds is of the order of 60% and above,[10] compound formation will result in large magnetic moments and a strong influence on the magnetic properties of the system even if the compounds form on a nanometer scale. An identification of intermetallic compounds in structural analysis therefore facilitates the interpretation of the magnetic properties of GeMn films. In particular, structural information is essential for films with Mn contents of a few percent,

where it may be difficult to unambiguously distinguish a magnetic semiconductor with intermetallic compounds from a diluted magnetic semiconductor.

In this work we provide new insights into the correlation of the magnetic and structural properties of $Ge_{0.95}Mn_{0.05}$ films fabricated with low temperature MBE. By carefully increasing the substrate temperature T_S from a temperature as low as 60°C, the onset of the formation of intermetallic compounds was determined. A combined transmission electron microscopy (TEM) and electron energy-loss spectroscopy (EELS) analysis identifies this compound formation with the precipitation of nanometer sized Mn_5Ge_3 inclusions. The amount and the size of these inclusions can be tuned with T_S without changing the Mn content of the samples. We therefore present the first systematic study of the influence of precipitation of Mn_5Ge_3 on the magnetic behaviour of $Ge_{0.95}Mn_{0.05}$ films. Magnetometry data reveal a superparamagnetic response of the precipitates between the ferromagnetic transition temperature $T_C^{Mn_5Ge_3}$ of Mn_5Ge_3 and a lower, characteristic temperature T_B, which depends on T_S and thus on the specific nanostructure of the samples. Below T_B, a blocking process occurs and provides nonzero magnetisation. At the lowest temperatures, the system shows the signature of a transition into a metastable state.

II. EXPERIMENTAL

GeMn films were fabricated in a RIBER SIVA 32 molecular beam epitaxy machine on intrinsic Ge(100) substrates. The substrates were cleaned *in situ* by annealing over at least 8 hours at a temperature of 400°C, followed by a 30 min annealing step at 600°C. A 100 nm intrinsic Ge buffer layer below the GeMn films provided an atomically flat and chemically clean surface. The GeMn films themselves were fabricated at substrate temperatures ranging from $T_S = 60$°C to $T_S = 120$°C to overcome the low Mn solubility in Ge of approximately 10^{-5} % in thermodynamic equilibrium.[11] A Ge rate of 0.08 Å/s was chosen to provide good crystalline quality. Mn was introduced by codeposition. All samples presented in this report have a manganese content of nominally 5 % and a GeMn layer thickness of 200 nm. The film quality was monitored *in situ* with reflection high energy electron diffraction (RHEED) and *ex situ* by TEM, x-ray diffraction (XRD) and atomic force microscopy (AFM).

The TEM analysis was carried out on a JEOL 3010 microscope operating at 300 kV. Samples were prepared by standard techniques using mechanical grinding, dimpling, and Ar ion-beam milling in a cold stage to avoid sample modifications due to unintentional thermal annealing. Cross-sections were prepared for samples fabricated at 60, 70, 100 and 120°C. EELS was used for the chemical analysis of the TEM samples. XRD $\theta - 2\theta$ scans were done with a commercial 40 kV x-ray diffractometer equipped with a Cu $K_{\alpha 1}$ cathode.

To investigate the magnetic properties of the films we employed DC and AC superconducting quantum interference device (SQUID) magnetometry with a QUANTUM DESIGN magnetometer. Several measurement procedures were applied to the samples to account for a possible dependence of the magnetic properties on the measurement history. If not otherwise stated, samples were measured during warmup from 2 to 350 K. Cooling procedures comprise cooling in the maximum available external field of $\mu_0 H = 7$ T (maximum field cooled, MFC), cooling in the measurement field (field cooled, FC) and cooling without external field (zero field cooled, ZFC). Different measurement fields were used for MFC measurements to extract field induced magnetic properties. Magnetisation loops were taken after maximum field cooldown to the measurement temperature. Both in sample plane and out of sample plane field directions were used.

III. STRUCTURAL PROPERTIES

RHEED patterns recorded after deposition of the buffer layer reveal perfect (2×1) reconstruction of the Ge surface. To investigate the influence of the low substrate temperatures on the surface reconstruction, we fabricated a reference sample without Mn codeposition at $T_S = 60$°C. The intensity of the RHEED patterns recorded after lowering the substrate temperature to
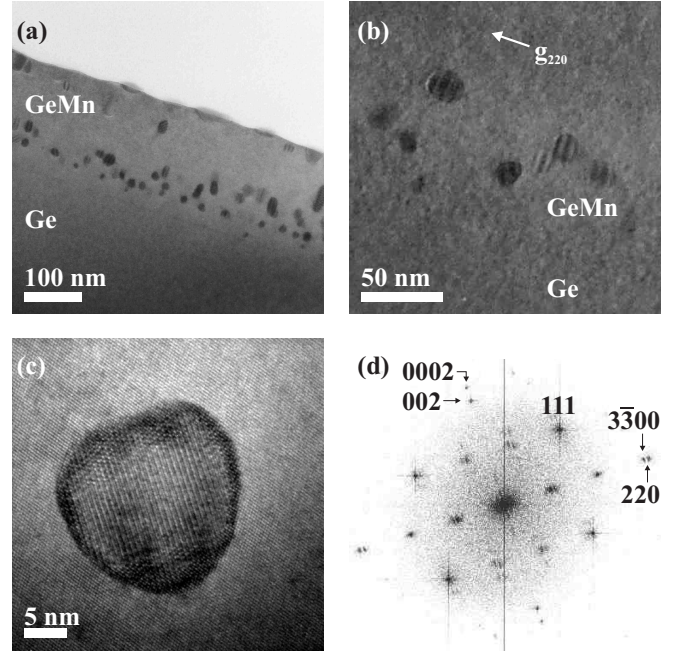

FIG. 1: Cross-sectional TEM micrographs of a sample with $T_S = 120$°C. (a) Bright-field cross-sectional TEM overview image. The dark regions correspond to Mn_5Ge_3 precipitates. (b) Typical Moiré fringe images of precipitates. (c) High-resolution TEM micrograph of a typical partially coherent precipitate. (d) Fourier transform of (c) showing cubic Ge and hexagonal Mn_5Ge_3 lattice reflection indices.

60°C weakens quickly within less than 5 nm of low temperature growth. In the following the intensity of the fundamental diffraction spots of the [110] azimuth stays at a constant level, while the [110] half-order diffraction spots disappear. AFM analysis of this reference sample reveals the formation of faceted pits within an otherwise flat surface. In contrary, samples with Mn codeposition exhibit streaky RHEED patterns characteristic for 2D island growth[12] for all substrate temperatures, indicating a suppressed pit formation. No pits were visible in AFM images and instead an island covered surface with a root mean square roughness of 1.5 nm was observed.

Bright-field cross-sectional TEM micrographs show that in spite of substrate temperatures below 120°C, high quality, dislocation free epitaxy can be achieved. Locally, however, inclusions are observed for $T_S \geq 70$°C as shown in Fig. 1(a) for the sample with $T_S = 120$°C. The dark regions in bright-field images of these samples correspond to inclusions in an unperturbed surrounding. For $T_S = 120$°C, typical inclusions are round with an average diameter of 10-20 nm.

The high-resolution (HR) TEM micrograph in Fig. 1(c) indicates a different crystal structure and/or orientation of these inclusions compared to the cubic matrix. The corresponding Fourier transform (FT) in Fig. 1(d) exhibits reflections in addition to the cubic Ge reflections which can be explained as part of a hexagonal pattern.

The intermetallic phase Mn_5Ge_3 is reported to be of hexagonal $D8_8$ structure.[13,14] Indeed, the FT pattern in Fig. 1(d) is in good agreement with the one expected for Mn_5Ge_3 films. The reflection indices in Fig. 1(d) represent the surrounding, cubic Ge matrix and in addition the reflexes of the hexagonal inclusions. Taking the Ge crystal lattice $a_{Ge} = 5.66\,\text{Å}$ as a reference, the lattice constants of the hexagonal inclusions are estimated as $a = 5.02 \pm 0.05\,\text{Å}$ and $c = 7.26 \pm 0.1\,\text{Å}$, which agree well within the error limits with the strain-free bulk values[14] of $a = 5.053\,\text{Å}$ and $c = 7.184\,\text{Å}$ for Mn_5Ge_3 films. Furthermore, $\theta - 2\theta$-XRD scans taken in the Ge (00ℓ) direction (not shown) reveal peaks that correspond to the (002) and (004) reflexes of bulk Mn_5Ge_3.[2,13] From TEM, XRD and the magnetometry results presented in Sec. IV the inclusions are identified as precipitation of intermetallic Mn_5Ge_3. Furthermore, a chemical analysis performed via EELS with a $10\,\text{nm}$ spot on the inclusions results in a very high Mn content for the inclusions, also indicating the presence of the intermetallic phase. In contrast, the Mn content in the matrix was found to be less than the detection limit of 1%. No sign of other intermetallic compounds was found by any of the employed characterisation techniques.

The orientation of the precipitates with respect to the Ge matrix is observed to be not random but showing the following topotaxial relation: $(0002)\,Mn_5Ge_3 \parallel (002)\,Ge$ and $\langle 11\bar{2}0 \rangle\,Mn_5Ge_3 \parallel \langle 110 \rangle\,Ge$, which agrees with recent results.[9] Due to the different crystal structures of the intermetallic precipitates and the Ge matrix, it is not possible to find parallel lattice planes along all crystal directions. The precipitates are therefore called partially coherent. It is remarkable that most of the precipitates appear in the same orientation relation to the matrix as demonstrated for $T_S = 120°C$ by the Moiré fringe image in Fig. 1(b) where the fringes are almost parallel for all precipitates. This results in a strong structural anisotropy regarding the distribution of the hexagonal c-axis of the precipitates compared to the growth direction.

For samples fabricated with $T_S < 120°C$ a different material contrast compared to Fig. 1 (a) is observed in bright-field TEM micrographs, as illustrated in Fig. 2(a) for $T_S = 70°C$. Features resembling the inclusions in Fig. 1(a) are marked with arrows. Their density and diameter is noticeably decreased. In addition to these features a slight contrast revealing elongated areas aligned along the growth direction arises. When selecting a characteristic reflex of the hexagonal Mn_5Ge_3 lattice in dark-field conditions in Fig. 2(b), only the inclusions are observed in bright contrast while the elongated areas disappear. The diameter of the inclusions is smaller than $9\,\text{nm}$. A HRTEM image of a typical inclusion is shown in Fig. 2(c). It has a hexagonal structure and is partially coherent with the matrix as the precipitates in Fig. 1. TEM analysis performed similarly to the sample with $T_S = 120°C$ identifies the inclusions as Mn_5Ge_3 precipitates.

The elongated regions aligned along the growth direc-
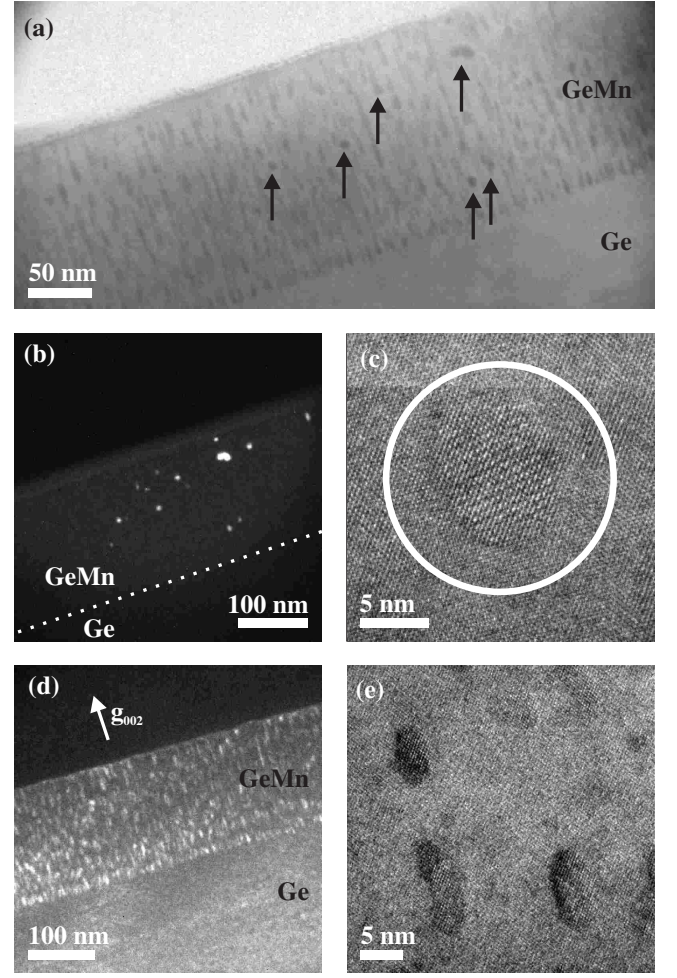

FIG. 2: Cross-sectional TEM micrographs of a sample with $T_S = 70°C$. (a) Bright field TEM overview image. Arrows mark Mn_5Ge_3 precipitates. (b) Dark-field TEM micrograph recorded after selecting a characteristic reflex of the hexagonal Mn_5Ge_3 lattice. The dashed line indicates the interface between GeMn layer and Ge buffer layer. Bright regions correspond to Mn_5Ge_3 precipitates. (c) High-resolution TEM of a partially coherent, hexagonal Mn_5Ge_3 precipitate, marked by the white circle. (d) Dark-field TEM micrograph recorded after selecting a characteristic reflex of the cubic Ge lattice. Bright regions represent the coherent clusters. (e) High-resolution TEM of typical coherent, cubic clusters.

tion can be visualized in dark-field conditions by selecting a chemically sensitive reflex of the Ge lattice as shown in Fig. 2(d) for the (002) reflex. They have typical diameters of $2-5\,\text{nm}$ and lengths of about ten nanometers. The round shaped Mn_5Ge_3 precipitates disappear, revealing a distinctly different composition and orientation relation for the elongated, bright areas. The contrast condition g_{002} that has to be chosen to observe the bright areas indicates that they represent regions of higher Mn content compared to the dark surrounding, the Mn being substitutionally incorporated on Ge sites. HRTEM micrographs of the sample presented in Fig. 2(e) show dark

regions that are similar to the bright regions both in size and shape. They can be identified with the bright areas of Fig. 2(d). These areas have a cubic structure and are a coherent part of the host matrix. The dark and bright areas of Fig. 2(d) represent areas of alternating low and high Mn concentration and thus an inhomogeneous dispersion of Mn in the Ge matrix. In the following, the bright areas of Fig. 2(d) will be denoted as clusters. EELS averaging over a 100 nm spot containing only coherent clusters results in an average Mn concentration of $\approx 5\%$, verifying the intended nominal stoichiometry of the $Ge_{0.95}Mn_{0.05}$ alloys. Since the cluster sizes are below the EELS resolution limit, no precise information on the Mn content of the individual clusters can be given. Nevertheless, an upper limit for the Mn content within the clusters can be deduced from the dark to bright contrast ratio in Fig. 2(d) and by assuming zero Mn content in the matrix, leading to a maximum Mn content in the bright areas of $\approx 15\%$.

TEM analysis shows that only the lowest substrate temperature sample produced at $T_S = 60°C$ exhibits no sign for intermetallic precipitates. It solely contains coherent clusters. The sample with $T_S = 70°C$ represents the sample with the lowest substrate temperature where a marginal amount of hexagonal precipitates can still be found as illustrated in Fig. 2 (a). TEM analysis on samples with $60°C < T_S \leq 120°C$ reveals an increasing amount and diameter of these precipitates, while in parallel the fraction of coherent clusters diminishes. At $T_S = 120°C$, only precipitates are present.

Hence, the variation of T_S in the epitaxy of $Ge_{0.95}Mn_{0.05}$ reveals the formation onset at $T_S = 70°C$ of the intermetallic compound Mn_5Ge_3 as well as the upper limit $T_S = 120°C$ for the dispersion of Mn in the Ge matrix. Under these epitaxy conditions, this random dispersion is not perfectly homogeneous, leading to the observation of clusters which are coherently bound to the surrounding and which show enhanced Mn content compared to the matrix. In contrast, the ferromagnetic Mn_5Ge_3 phase appears in form of unstrained small precipitates. Both precipitates and clusters can be present in one and the same sample and are thus expected to influence the magnetic properties of the $Ge_{0.95}Mn_{0.05}$ films, which are investigated in the following section.

IV. MAGNETIC PROPERTIES

Fig. 3 shows the magnetisation of the several $Ge_{0.95}Mn_{0.05}$ films measured versus temperature. The curves were measured in different applied magnetic fields after cooling down in zero field (ZFC), the measurement field (FC) or the maximum available field of $\mu_0H = 7\,T$ (MFC). Bulk Mn_5Ge_3 is reported[15] to be ferromagnetic below $T_C^{Mn_5Ge_3} = 296\,K$ and to be characterised by a magnetisation versus temperature curve shape similar to the one observed for the $T_S = 120°C$ sample, which, according to Sec. III, contains only Mn_5Ge_3 precipitates.
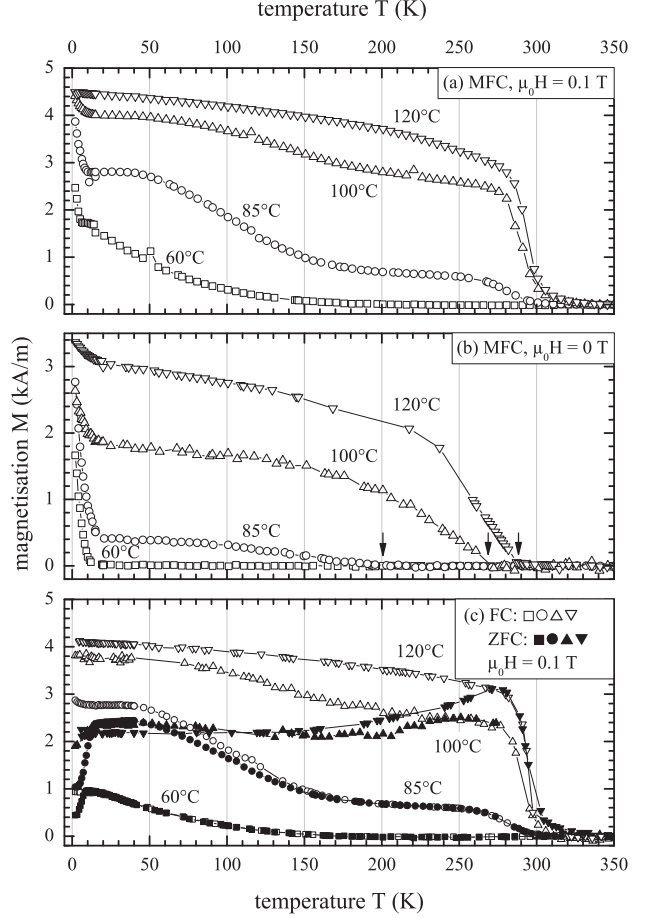

FIG. 3: Magnetisation versus temperature curves of samples fabricated with substrate temperatures T_S between 60 and 120°C. External fields were applied in the sample plane. Magnetisation was measured during warmup. (a) MFC, $\mu_0H = 0.1\,T$. (b) MFC, $\mu_0H = 0\,T$. The arrows indicate the onset of magnetisation. (c) Field cooled (FC, open symbols) and zero field cooled (ZFC, closed symbols) measurements, $\mu_0H = 0.1\,T$.

Therefore the magnetisation onset in Fig. 3(a) near room temperature is interpreted as the paramagnetic to ferromagnetic transition of the individual Mn_5Ge_3 precipitates at $T_C^{Mn_5Ge_3}$. For all samples containing precipitates, that is samples with $T_S > 60°C$, a nonzero magnetic signal arises in the $\mu_0H = 0.1\,T$ MFC measurement of Fig. 3(a) below $T_C^{Mn_5Ge_3}$. Switching off the external field in Fig. 3(b) reveals that this behaviour is field induced. The onset of magnetisation now significantly shifts to a lower, T_S dependent, characteristic temperature. This temperature, marked by the arrows in Fig. 3(b), will hereafter be denoted as T_B.

In contrast to this, the precipitate-free $T_S = 60°C$ sample containing only coherent clusters does not show a field induced magnetic signal at $T_C^{Mn_5Ge_3}$ in Fig. 3(a). In the absence of an external field, there is no measurable magnetisation in Fig. 3(b) above approximately 18 K. Instead, the magnetic signature of the coherent clusters is

a field induced magnetisation up to approximately $200\,\mathrm{K}$ as shown in Fig. 3(a). Therefore, the contribution of the coherent clusters on the magnetisation versus temperature curves for $60°\mathrm{C} < T_{\mathrm{S}} < 120°\mathrm{C}$ can be experimentally separated from the contribution of the precipitates by examining the precipitate-free $T_{\mathrm{S}} = 60°\mathrm{C}$ sample.

In FC / ZFC measurements in Fig. 3(c), samples with $T_{\mathrm{S}} > 60°\mathrm{C}$ exhibit a peak in the ZFC curve and a bifurcation of FC and ZFC curves slightly below the position of the peak in the ZFC magnetisation curve. The ZFC peak position coincides with T_{B}. For the $T_{\mathrm{S}} = 60°\mathrm{C}$ sample, no peak or bifurcation at all is found at high temperatures. The $T_{\mathrm{S}} = 85°\mathrm{C}$ sample in turn exhibits a bifurcation of FC and ZFC curves, but no peak at T_{B} in the ZFC curve.

In the measurements of Fig. 3(a) and (b), a pronounced, steep increase of magnetisation is visible for samples with $T_{\mathrm{S}} < 120°\mathrm{C}$ below approximately $18\,\mathrm{K}$. In the same temperature region, a drop of the ZFC signal compared to a plateau-like curve form of the FC signal is observed in Fig. 3(c) for these samples. The steep increase in magnetisation is the only deviation for the $T_{\mathrm{S}} = 60°\mathrm{C}$ sample from the zero magnetisation in Fig. 3(b). A thorough analysis of the precipitate-free $T_{\mathrm{S}} = 60°\mathrm{C}$ sample reveals that this behaviour can be interpreted as a magnetic signature of the coherent clusters.[16]

The real part of the AC susceptibility of the $T_{\mathrm{S}} = 85°\mathrm{C}$ sample presented in Fig. 4 shows two well separated peaks, one at low temperatures, and one which coincides with the characteristic temperature T_{B}. While the first one at low temperatures is also present for the precipitate-free $T_{\mathrm{S}} = 60°\mathrm{C}$ sample, the latter is not visible in that sample. Furthermore, the second peak is the only observable peak in the $T_{\mathrm{S}} = 120°\mathrm{C}$ sample which solely contains precipitates, so that we attribute the second peak to the presence of $\mathrm{Mn_5Ge_3}$ precipitates, and the first peak to the presence of coherent clusters. The high temperature peak occurs significantly below $T_{\mathrm{C}}^{\mathrm{Mn_5Ge_3}}$ for $T_{\mathrm{S}} = 85°\mathrm{C}$ and slightly below $T_{\mathrm{C}}^{\mathrm{Mn_5Ge_3}}$ for $T_{\mathrm{S}} = 120°\mathrm{C}$, ruling out a correlation to a $\mathrm{Mn_5Ge_3}$ paramagnetic to ferromagnetic transition. The peak position shifts with the measurement frequency, as shown in the inset of Fig. 4.

V. DISCUSSION

The magnetic characterisation of the samples shown in Fig. 3 reveals three different temperature regimes. The first regime begins with a field induced onset of magnetisation at $T_{\mathrm{C}}^{\mathrm{Mn_5Ge_3}}$ in the presence of an external field, as shown in Fig. 3(a). The second regime is marked by the onset of magnetisation at T_{B} below $T_{\mathrm{C}}^{\mathrm{Mn_5Ge_3}}$ in the absence of an external field, as indicated by the arrows in Fig. 3(b). The third regime is found at low temperatures, where a steep increase of magnetisation towards lower temperatures is observed both in Figs. 3(a) and (b). Each of these temperature regions will be discussed
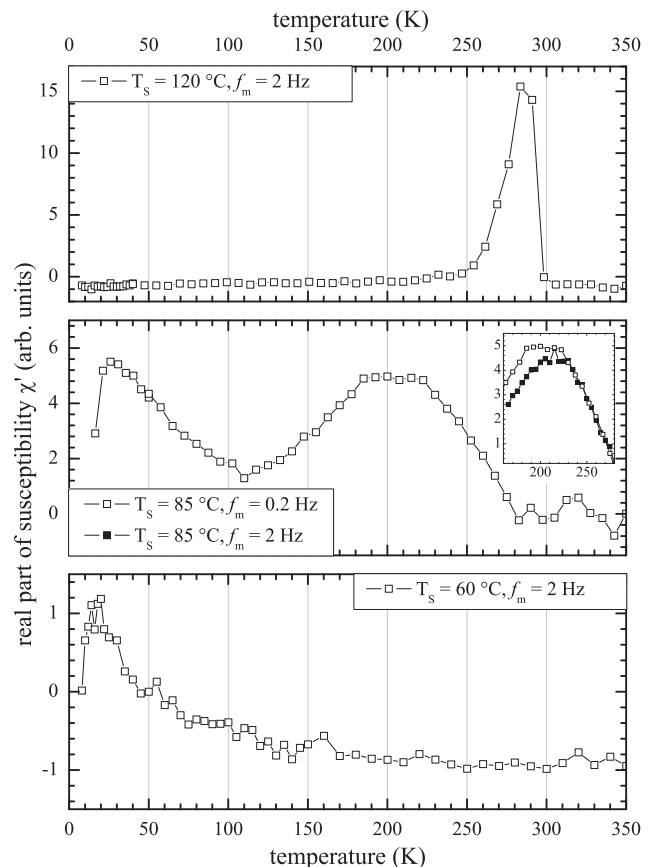

FIG. 4: Real part of the AC susceptibility versus temperature. The measurement field $\mu_0\mathrm{H} = 0.5\,\mathrm{mT}$ was applied perpendicular to the sample plane. (inset) Shift of the AC susceptibility peak with measurement frequency towards higher temperatures, shown for a sample with $T_{\mathrm{S}} = 85°\mathrm{C}$.

separately in the following subsections.

A. Superparamagnetic regime

The highest relevant temperature involved in a complete description of the magnetic properties of samples with $T_{\mathrm{S}} > 60°\mathrm{C}$ is the Curie temperature of $\mathrm{Mn_5Ge_3}$, i.e. $T_{\mathrm{C}}^{\mathrm{Mn_5Ge_3}} = 296\,\mathrm{K}$.[15] At this temperature, the individual $\mathrm{Mn_5Ge_3}$ precipitates turn ferromagnetic and carry large magnetic moments. The typical diameter of the precipitates observed in the TEM analysis of Sec. III is reasonably smaller than the roughly estimated critical value[17] of $15\,\mathrm{nm}$ to display single domain behaviour. Therefore, below $T_{\mathrm{C}}^{\mathrm{Mn_5Ge_3}}$, the precipitates are expected to react freely on an externally applied field like a paramagnet with large magnetic moment, that is like a superparamagnet. A consequence of the superparamagnetic response of the samples on an applied field is the field induced magnetisation revealed in the magnetisation versus temperature curves of Fig. 3. This field induced behaviour is reversible, so that MFC, FC and ZFC measurements co-
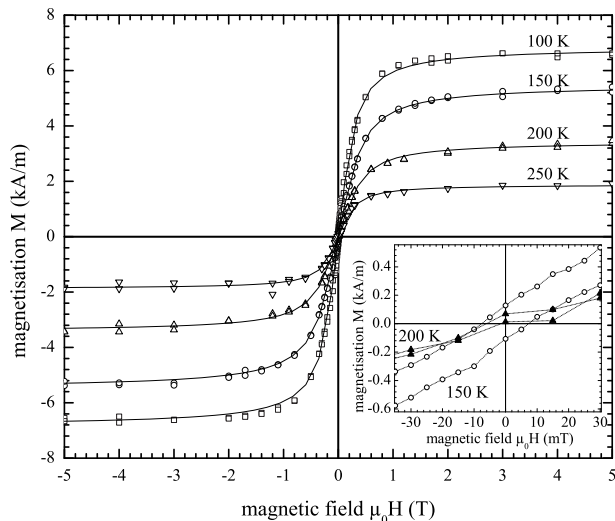
FIG. 5: Magnetisation curves taken for a $T_S = 85°C$ sample with external field applied in plane of the sample. Solid lines represent Langevin fits. (inset) Closeup of the same dataset. Hysteresis effects gradually appear below 200 K.

incide. Reversibility also results in the disappearance of hysteresis in magnetisation loops. These loops can then be described by a superparamagnetic Langevin function $L(y)$, so that

$$\begin{aligned} M(y) &= M_S L(y) \\ &= M_S \left(\coth y - \frac{1}{y} \right) \ , \ y = \frac{\mu \mu_0 H}{k_B T} \end{aligned} \quad (1)$$

with M_S being the saturation magnetisation and μ the magnetic moment of the particles. This is shown in Fig. 5 at $T = 200$ K and $T = 250$ K for the sample with $T_S = 85°C$. The Langevin fit at these temperatures results in magnetic moments of the order of $\mu = 2000\mu_B$. The superparamagnetic regime extends down to T_B, in case of the $T_S = 85°C$ sample down to $T_B = 205$ K. Below T_B, a blocking process discussed in the following subsection occurs.

B. Blocking regime

Bulk Mn_5Ge_3 is reported to exhibit uniaxial magnetic anisotropy with respect to its c-axis.[18,19] The presence of such a magnetic anisotropy in an assembly of superparamagnetic fine particles leads to the existence of an anisotropy energy barrier E_A,

$$E_A = KV \sin^2(\theta) \quad (2)$$

with K being the anisotropy energy density, V the particle volume and θ the angle between magnetic moment and anisotropy axis.[20] The energy barrier does not affect the system at the comparably high temperatures of the superparamagnetic regime, where the anisotropy energy

barrier is smaller than the thermal energy and hence is easily overcome by thermal activation. However, if the temperature is lowered below a characteristic blocking temperature T_B, the energy barrier blocks the magnetic moments in a direction either parallel or antiparallel to the anisotropy axis.

According to the theory of Néel and Brown, the direction of magnetisation of superparamagnetic particles undergoes a sort of Brownian motion.[20] In the presence of an energy barrier, these thermal fluctuations take place with a relaxation rate that is given by

$$f = f_0 \exp \left(- \frac{KV}{k_B T} \right). \quad (3)$$

f_0 is a typical attempt frequency of the order of 10^9 Hz.[21,22] With decreasing temperature the fluctuations slow down until the magnetic moments eventually become stable below the temperature T_B on the characteristic time scale $1/f$ of an experiment. The associated temperature is denoted as the blocking temperature T_B. An AC susceptibility experiment with a measurement frequency f_m directly probes this blocking process. A peak in the measured susceptibility versus temperature curve is expected for the temperature T_B where the measurement frequency f_m is equal to the fluctuation frequency f. According to this model different measurement frequencies are associated with different values of T_B. Hence, a shift of the peak position in the susceptibility versus temperature curves is obtained as shown in the inset of Fig. 4 for a sample with $T_S = 85°C$. The measured value of the relative shift per frequency decade,

$$\frac{\Delta T_B}{T_B \Delta \log f} \quad (4)$$

equals 0.075 and is close to the value of 0.1 typically observed in superparamagnetic systems. Following Bean and Livingston,[23] the thermal fluctuations can be considered as stable if the relaxation time of the fluctuations $\tau = 1/f$ is of the order of 10^2 s, that is, if

$$25k_B T_B = KV. \quad (5)$$

Employing the particle dimensions found in the TEM analysis of Sec. III and assuming a spherical particle shape in Eq. (5), we can estimate values for the anisotropy constant K of the precipitates from the blocking temperatures observed in Fig. 3(b). The results of this analysis are summarised in Tab. I.

In the $\mu_0 H = 0$ T MFC measurements in Fig. 3(b), the precipitate moments are aligned by the maximum field cooldown. Below T_B, they are blocked by the anisotropy energy barrier on the typical time scale of the experiment, so that their magnetic behaviour is no longer reversible and an overall nonzero magnetisation is observable. As shown in Tab. I, T_B increases with increasing T_S and thus with increasing precipitate diameter. The blocking process itself does not provide a spontaneous overall magnetisation, as parallel or antiparallel alignment of the

TABLE I: Blocking temperatures for samples with precipitates extracted from the measurements of Fig. 3, mean precipitate diameter and estimated anisotropy constant K.

T_S	70°C	85°C	100°C	120°C
T_B in K (from Fig. 3(b))	118^a	205	269	287
T_B in K (from Fig. 3(c))	-	198	258	278
mean diameter in nm (TEM)	9.0	-	11.4	13.6
K^b in 10^6 erg/cm^3	1.1	-	1.2	0.8

^{a}not shown in Fig. 3
^{b}obtained from Eq. (5) with T_B values of Fig. 3(b)

magnetic moments with respect to the anisotropy axis is equally probable.[24] This is observed when magnetisation is measured during zero field cooldown (not shown), where no overall nonzero magnetisation is detected. The absence of reversibility below T_B results in a bifurcation of FC and ZFC curves below T_B, as well as in a peak at T_B in ZFC measurements in Fig. 3(c). Hysteresis effects gradually arising below T_B are a further consequence of the blocking of the magnetic supermoments. This is shown in the inset of Fig. 5 for a $T_S = 85$°C sample with $T_B = 205$ K.

For each substrate temperature the TEM analysis reveals a certain precipitate size distribution. Due to the correlation of precipitate volume and blocking temperature, this results in a broad temperature range of the blocking process and thus in a broad peak around an average T_B in the AC susceptibility measurements. For the sample with $T_S = 85$°C, this peak expands between approximately 100 and 275 K as shown in Fig. 4. The broad temperature range of the blocking process leads to a situation where, depending on the individual particle volume, both blocked and unblocked moments are present at a given temperature close to the experimentally observed average T_B. This explains why physically reasonable Langevin fits of the reversible part of the magnetisation loops in Fig. 5 can be performed below $T_B = 205$ K down to 100 K. The deduced magnetic moments range from $1200\,\mu_B$ at 100 K to $2900\,\mu_B$ at 250 K and increase with measurement temperature. Larger particles are blocked up to higher temperatures, so that for lower temperatures only the smaller particles are probed by the Langevin function and smaller magnetic moments are found. To observe temperature independent magnetic supermoments in magnetisation loops, measurements would have to be performed at temperatures well above the blocking temperature, which is hindered by $T_C^{\mathrm{Mn_5Ge_3}}$ naturally setting a limit to the superparamagnetic regime.

In samples that contain both clusters and precipitates, that is for 60°C $< T_S < 120$°C, the magnetic signal of the coherent clusters is overlaid over the magnetic signature of the intermetallic precipitates. In an externally applied field as in Fig. 3(a), this results in magnetisation versus temperature curves that can be regarded as a superposition of those obtained for the $T_S = 60$°C sample and the ones obtained for higher T_S samples. Also the temperature of the magnetisation onset of the $T_S = 60$°C sample is visible in the higher T_S samples as a shoulder in the magnetisation versus temperature curves. The height of this shoulder decreases with T_S, since the coherent cluster content decreases with higher substrate temperatures, as discussed in Sec. III. Without an external field as in Fig. 3(b), only the signal coming from the Mn$_5$Ge$_3$ precipitates is observable above 18 K, since the clusters do not exhibit an overall nonzero magnetic signal in zero field conditions. The $T_S = 85$°C sample contains considerable amounts of both coherent clusters and Mn$_5$Ge$_3$ precipitates. The peak at T_B in the ZFC measurements of Fig. 3c is suppressed for this sample, while it is pronounced for samples with higher T_S and therefore lower cluster content. We interpret this suppression to result from the ZFC curve for $T_S = 120$°C, characteristic for the contribution of the precipitates, being overlaid by the ZFC curve for $T_S = 60$°C, characteristic for the clusters.

C. Metastable regime

For temperatures below 18 K, the precipitate-free $T_S = 60$°C sample exhibits magnetic signatures of a transition into a metastable state, which we proposed[16] to be a consequence of the formation of coherent clusters. These magnetic signatures are observed for samples with $T_S > 60$°C in the same temperature range. They appear as a drop of the ZFC signal at low temperatures compared to a plateau-like curve form of the FC signal of Fig. 3(c), and as a steep increase in the MFC measurements of Fig. 3(a) and (b). Furthermore, magnetisation relaxation in time dependent measurements (not shown) and a peak in the AC susceptibility, as shown in Fig. 4, occur at this temperature range. This behaviour is visible for all samples containing coherent clusters and gets more and more suppressed as T_S is increased, that is as the amount of coherent clusters in the films is reduced. From this trend we conclude that the features characteristic of a metastable state observed for samples with $T_S > 60$°C are due to the presence of the inhomogeneous dispersion of Mn in the Ge matrix.

VI. CONCLUSION

In conclusion, we have presented a study of the magnetic and structural properties of Ge$_{0.95}$Mn$_{0.05}$ films fabricated by low temperature MBE at substrate temperatures T_S ranging from 60°C to 120°C. An extensive TEM analysis reveals the precipitation of nanometer sized intermetallic Mn$_5$Ge$_3$ compounds for substrate temperatures $T_S \geq 70$°C. The amount and size of these inclusions can be tuned with the substrate temperature without changing the Mn content of the samples. Precipitation can be suppressed at $T_S = 60$°C. Therefore, we were able to systematically investigate and iden-

tify the influence of precipitation on the magnetic behaviour of the films. The magnetic signature of the precipitates is a field induced, superparamagnetic signal between the ferromagnetic transition temperature $T_{\mathrm{C}}^{\mathrm{Mn_5Ge_3}} = 296\,\mathrm{K}$ of $\mathrm{Mn_5Ge_3}$ and a lower, characteristic temperature T_{B}. Below T_{B}, nonzero magnetisation in the absence of an external field, as well as hysteresis in magnetisation loops is observed, which is due to a blocking process of the superparamagnetic precipitates. Therefore our study indicates that reports on hysteresis in magnetisation loops[7,8] and a field induced magnetisation onset near room temperature[4] in possibly diluted magnetic semiconductors might be a result of the presence of precipitates in the films. At low temperatures, samples with $70°\mathrm{C} \leq T_{\mathrm{S}} < 120°\mathrm{C}$ undergo a transition into a metastable state that is interpreted as a signature of an inhomogeneous Mn dispersion in the Ge matrix observed in addition to the precipitates.

[1] J.-S. Kang, G. Kim, S. C. Wi, S. S. Lee, S. Choi, S. Cho, S. W. Han, K. H. Kim, H. J. Song, H. J. Shin, et al., Phys. Rev. Lett. **94**, 147202 (2005).

[2] C. G. Zeng, S. C. Erwin, L. C. Feldman, A. P. Li, R. Jin, Y. Song, J. R. Thompson, and H. H. Weitering, Appl. Phys. Lett. **83**, 5002 (2003).

[3] Y. D. Park, A. Wilson, A. T. Hanbicki, J. E. Mattson, T. Ambrose, and G. Spanos, Appl. Phys. Lett. **78**, 2739 (2001).

[4] Y. D. Park, A. T. Hanbicki, S. C. Erwin, C. S. Hellberg, J. M. Sullivan, J. E. Mattson, T. F. Ambrose, A. Wilson, G. Spanos, and B. T. Jonker, Science **295**, 651 (2002).

[5] A. P. Li, J. Shen, J. R. Thompson, and H. H. Weitering, Appl. Phys. Lett. **86**, 152507 (2005).

[6] A. P. Li, J. F. Wendelken, J. Shen, L. C. Feldman, J. R. Thompson, and H. H. Weitering, Phys. Rev. B **72**, 195205 (2005).

[7] F. D'Orazio, F. Lucari, N. Pinto, L. Morresi, and R. Murri, J. Magn. Magn. Mater. **272-276**, 2006 (2004).

[8] N. Pinto, L. Morresi, M. Ficcadenti, R. Murri, F. D'Orazio, F. Lucari, L. Boarino, and G. Amato, Phys. Rev. B **72**, 165203 (2005).

[9] C. Bihler, C. Jaeger, T. Vallaitis, M. Gjukic, M. S. Brandt, E. Pippel, J. Woltersdorf, and U. Gösele, Appl. Phys. Lett. **88**, 112506 (2006).

[10] B. Predel, in *Landolt-Börnstein - Group IV: Physical Chemistry* (Springer, Berlin, Heidelberg, 1996), vol. 5.

[11] A. Mühlbauer, in *Landolt-Börnstein - Group III: Crystal and Solid State Physics* (Springer, Berlin, Heidelberg, New York, Tokio, 1984), vol. 17/C.

[12] K. A. Bratland, Y. L. Foo, J. A. N. T. Soares, T. Spila, P. Desjardins, and J. E. Greene, Phys. Rev. B **67**, 125322 (2003).

[13] L. Castelliz, Monatsh. Chem. / Chem. Monthly **84**, 765 (1953).

[14] J. B. Forsyth and P. J. Brown, J. Phys.: Condens. Matter **2**, 2713 (1990).

[15] N. Yamada, J. Phys. Soc. Jpn. **59**, 273 (1990).

[16] D. Bougeard, S. Ahlers, A. Trampert, N. Sircar, and G. Abstreiter (2006), unpublished.

[17] C. Kittel, Phys. Rev. **70**, 965 (1946).

[18] Y. Tawara and K. Sato, J. Phys. Soc. Jpn. **18**, 773 (1963).

[19] S. Picozzi, A. Continenza, and A. J. Freeman, Phys. Rev. B **70**, 235205 (2004).

[20] I. S. Jacobs and C. P. Bean, in *Magnetism*, edited by G. T. Rado and H. Suhl (Academic Press, New York, London, 1963), vol. III.

[21] W. F. Brown, Jr., Phys. Rev. **130**, 1677 (1963).

[22] W. F. Brown, Jr., J. Appl. Phys. **30**, S130 (1959).

[23] C. P. Bean and J. D. Livingston, J. Appl. Phys. **30**, S120 (1959).

[24] J. Hesse, H. Bremers, O. Hupe, M. Veith, E. W. Fritscher, and K. Valtchev, J. Magn. Magn. Mater. **212**, 153 (2000).